scientific reports

Check for updates

OPEN

Coenzyme Q10 protects keratinocytes against oxidation-induced energy stress as revealed by spatiotemporal analysis of cell energetics

Roland Abi Nahed[1]✉, Ali Hussein[1], Cécile Cottet-Rousselle[1], Alexandra Vogelsang[2], Francesco Aulicino[3], Imre Berger[3], Thomas Blatt[2], Julia M. Weise[2] & Uwe Schlattner[4]✉

Coenzyme Q10 (Q10) plays a critical role in cellular energy conversion within the mitochondrial respiratory chain and offers protective effects against oxidative and metabolic stress. In this study, we investigated the impact of Q10 on the spatio-temporal patterns of cellular energetics in keratinocyte-derived HaCaT cells, utilizing the genetically-encoded FRET sensor AMPfret. Engineered from the AMP-activated protein kinase (AMPK), this sensor leverages endogenous affinities of the kinase that evolved to detect energy stress, specifically decreases in ATP/ADP and ATP/AMP ratios that pose a threat to cell survival. We successfully established HaCaT cells stably expressing AMPfret, validated their functionality by inducing energy stress with 2-deoxy-D-glucose, and demonstrated that Q10, together with high glucose conditions in culture, can enhance cellular energetics compared to low glucose controls. We then employed AMPfret to analyze the spatio-temporal response of HaCaT keratinocytes to Luperox (tert-butyl peroxide), a potent organic prooxidant, in the presence of varying intracellular levels of Q10. Preloading cells with Q10 was protective, slowing the speed and reducing the extend of the energy stress response. In contrast, preincubation with Simvastatin, an inhibitor of the mevalonate Q10 biosynthesis pathway, depleted cellular Q10 levels, accelerated the onset of energy stress, and led to early cell death as compared to controls. Under all conditions, AMPfret revealed cell-to-cell heterogeneity in energy stress at baseline and in the response to Luperox. Overall, tracking changes in energy state in time and at single-cell level allows further insights into the beneficial role of Q10 in enhancing cellular bioenergetics in skin cells, and a potential role of AMPK in mediating responses to altered Q10 levels.

Keywords Coenzyme Q10, FRET sensor, Keratinocytes, HaCaT cells, Cellular bioenergetics, Oxidative stress

Coenzyme Q10 (Q10), also known as ubiquinone, is a lipid-soluble molecule that plays a fundamental role in cellular metabolism, particularly in mitochondrial energy conversion and protection against oxidative damage[1]. Within the complex network of cellular functions, mitochondrial ATP generation is crucial, as it powers nearly every biochemical reaction essential for life[2]. ATP generation through oxidative phosphorylation depends on the efficient operation of the electron transfer system (ETS) in the inner mitochondrial membrane. Within the ETS, different electron transfer pathways, including complex I and complex II, converge to the Q10 pool as a crucial and central electron carrier. Q10 then delivers its electrons to complex III for the final oxidative reaction in complex IV, thus supporting the generation of the electrochemical proton gradient for the synthesis of ATP[3,4]. In addition, as a potent antioxidant present in biological membranes, Q10 as ubiquinol can neutralize reactive oxygen species (ROS) in the mitochondria, which are natural byproducts of ETS function. It also plays a role

[1]Univ. Grenoble Alpes, INSERM U1055, Laboratory of Fundamental and Applied Bioenergetics (LBFA), 2280 Rue de La Piscine, 38058 Grenoble, France. [2]Research and Development, Beiersdorf AG, 20245 Hamburg, Germany. [3]Bristol Synthetic Biology Centre BrisSynBio, Biomedical Sciences, School of Biochemistry, University of Bristol, 1 Tankard's Close, Bristol BSH 1TD, UK. [4]Univ. Grenoble Alpes, INSERM U1055, InstitutUniversitaire de France, Laboratory of Fundamental and Applied Bioenergetics (LBFA), 2280 Rue de La Piscine, 38058 Grenoble, France. ✉email: rolandabinahed@gmail.com; uwe.schlattner@univ-grenoble-alpes.fr

in the plasma membrane redox system, protecting cell membranes from lipid peroxidation. Exerting this dual function in cell metabolism Q10 can prevent oxidative damage to various cellular components[5,6].

The potential therapeutic applications of Q10 have garnered significant attention, particularly in the context of diseases characterized by mitochondrial dysfunction and oxidative stress[7–10]. This includes cardiovascular diseases[11,12], neurodegenerative disorders such as Parkinson's disease[13], the metabolic syndrome[14], or more specific mitochondrial diseases, in particular mitochondrial respiratory chain disorders that are extremely difficult to treat. It also includes damaged skin, affecting its barrier function in protecting from environmental stressors such UV radiation, chemicals or environmental pollutants[15,16]. In particular, UV radiation generates ROS in skin cells and is a major factor for accelerated skin aging. As skin ages, endogenous Q10 level decline[17]. In addition, Q10 itself is an UV-sensitive molecule[18]. Thus, topical Q10 supplementation is commonly used as an anti-aging skin care approach[19], whereas oral Q10 administration could be a valuable addition to treatment strategies aimed at managing all the systemic conditions[20].

Energy stress, a condition characterized by reduced absolute ATP levels and relative ATP/ADP and ATP/AMP ratios, is a major parameter for cellular dysfunction and often leads to cell death if not properly managed. Such energy imbalance can result from a large mismatch between cellular energy intake and energy expenditure as occurring during nutrient deprivation or strenuous exercise, or specific pathological or stress conditions that lead to mitochondrial dysfunction and impaired cellular respiration. Under these conditions, cells activate a range of stress response pathways aimed at restoring energy balance and protecting against energy decreases and further cellular damage. However, if energy stress persists, cells can overcome these protective mechanisms, leading to a cascade of deleterious effects, including impaired cellular functions, oxidative stress, and eventually apoptosis or necrosis[21].

In recent years, the development of genetically-encoded, fluorescent biosensors provided powerful tools for real-time monitoring of cell metabolism in space and time[22–28]. Recent advancements in such biosensor technology have demonstrated new insights into the real-time dynamics of cellular energy states and stress responses[23–27,29–32]. AMPfret technology utilizes fluorescence resonance energy transfer (FRET) to track changes in ATP/ADP and ATP/AMP ratios within living cells[22–24,26]. The sensor was engineered based on the AMP-activated protein kinase (AMPK) fused to two fluorescent proteins, CFP and Venus. The distance between these two fluorophores decreases when AMPK switches from the inactive ATP-bound to the active ADP- or AMP-bound state. In contrast to other available ATP or ATP/ADP sensors, AMPfret leverages the natural affinity of AMPK that evolved for the detection of a critical threshold energy stress, i.e. ATP/ADP and ATP/AMP ratios that could potentially threaten cell survival. AMPfret already offered valuable insights into the mechanisms of AMPK activation and physiologically relevant cellular energy dynamics[22–24,26].

This study aimed to explore the impact of Q10 on the spatio-temporal pattern of cellular energy state in HaCaT skin cells. It specifically analyzed conditions of oxidative stress induced by Luperox (tert-butyl peroxide), a strong prooxidant, using AMPfret as a main readout. Our results reveal the primordial role of intracellular Q10 levels in the cellular capacity to respond to a large oxidative insult, but also the cell-to-cell variability underlying cell culture experiments. Such biosensor analysis enables a rapid and more comprehensive assessment of cellular energy stress responses, making it as a powerful tool for evaluating cellular stress responses.

Results

HaCaT keratinocyte cell line stably expressing AMPfret faithfully report energy stress

To obtain cells with reproducible and appropriate expression levels of the AMPfret energy sensor, we generated a HaCaT cell line stably expressing all sensor components. Since AMPfret is encoded by three different genes[23], we designed two lentiviruses that harbor either AMPKα2-CFP alone or both AMPKβ2-mVenus and AMPKγ1. HaCaT cells infected with these two lentiviruses were grown under selective conditions and subjected to limited dilution to select AMPfret expressing clones. The selected HaCaT clone 1 (HaCaT C1) shows well detectable CFP and mVenus fluorescence homogeneously distributed within the cytosol, revealing expression of the corresponding fusion proteins (Fig. 1a). In addition, excitation of CFP also yielded emission of mVenus fluorescence, i.e. a FRET signal (Fig. 1a), showing that both AMPKα2-CFP and AMPKβ2-mVenus subunits were present in the same complex. Immunoblotting confirmed stoichiometric levels of AMPKα2-CFP (88 kDa) and AMPKβ2-mVenus (57 kDa) subunits, together with AMPKγ1 (37 kDa) in these HaCaT C1 cells (Fig. 1b and Suppl. Figure 1a-d), despite the distribution of the genes in two different lentiviruses. As a functional control, we tested the response of these HaCaT C1 cells to inhibition of glycolysis by 20 mM 2-deoxy-D-glucose (2-DG)[33,34]. In this model, the normalized FRET ratio of AMPfret (Fig. 1c, d), herein called AMPfret signal, increased with time as the inhibitory effect set in, reaching a maximum after about 70–80 min. This reflects the energy stress, i.e. the decreased ATP/ADP (Fig. 1e) and ATP/AMP ratios, which are major activating signals of the AMPK pathway. At the end of our observation period, the AMPfret signal remained stable, indicating that cellular energy state was not further deteriorated (Fig. 1c). This is likely a direct consequence of AMPK activation, which triggers cellular processes that compensate for the loss in ATP, thus limiting further decline of cellular energy state. These data demonstrate the correct functioning of our sensor and indicate that HaCaT C1 cells largely rely on glycolysis for ATP generation. However, they are capable of preventing an excessive loss of ATP during the first 90 min of exposure to glycolysis inhibitor and show only slightly reduced viability (8%; Suppl. Figure 1e) without morphological indications of cell death (Fig. 1d).

Combined Q10 preincubation and high glucose increase keratinocyte energy state

We then examined under which growth conditions a preincubation with Q10 in DMEM can yield maximal effects on key parameters of HaCaT C1 energy state: the ATP/ADP ratio (Fig. 2a), the ATP/AMP ratio (Fig. 2b), and the adenylate energy charge (Ref.[35]; Fig. 2c), quantified by HPLC. When cultured for 1 h under low glucose conditions (1 g/L, control), 72 h preincubation with Q10 did not alter these energy parameters, and also addition

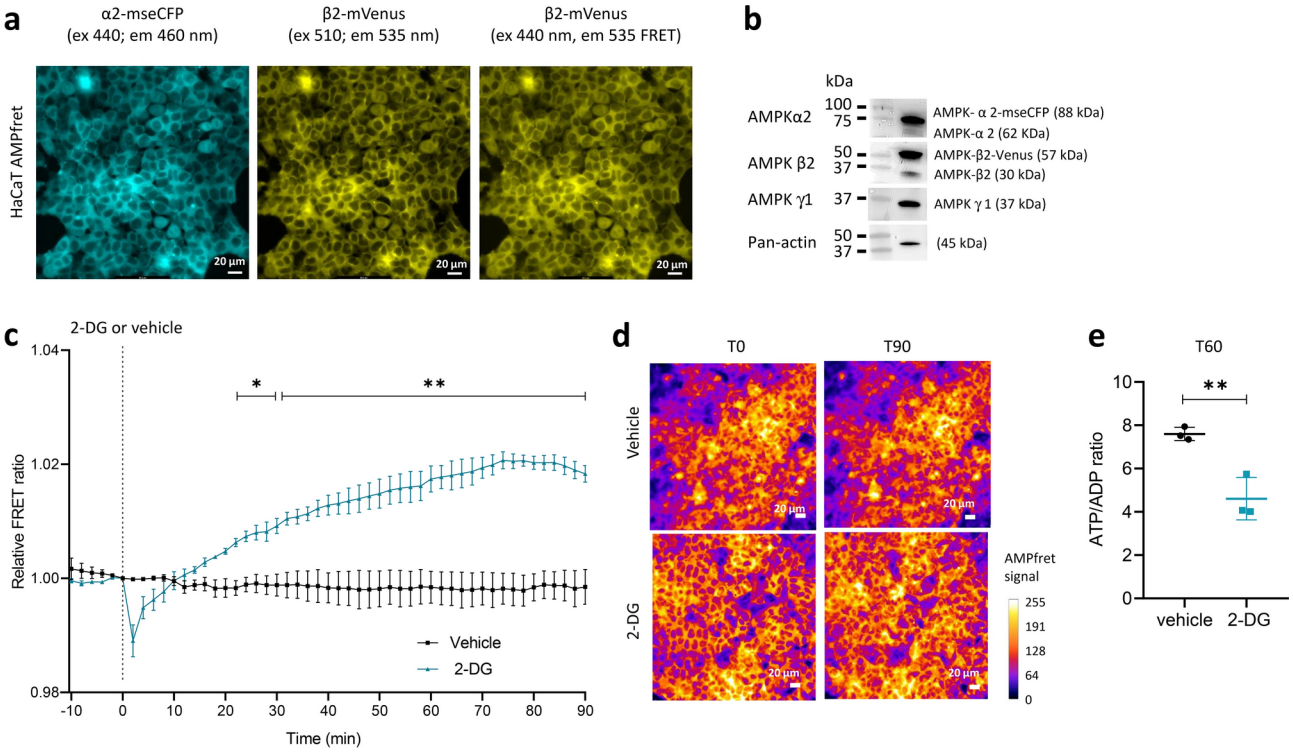

Fig. 1. Stable, functional AMPfret expression in HaCaT C1 keratinocytes. (**a**) Epifluorescence microscopy images of HaCaT C1 cells showing fluorescence at specific excitation (ex) and emission (em) wavelengths for CFP (ex: 440 nm, em: 460 nm, blue), Venus (ex: 510 nm, em: 535 nm, yellow) and the FRET channel (ex: 440 nm, em: 535 nm, yellow). (**b**) Representative immunoblots showing the expression of endogenous AMPK and AMPfret AMPK subunits in HaCaT C1 cells (two independent experiments; for uncropped immunoblots, refer to Suppl. Figure 1a-d). (**c**) Time course of normalized FRET ratio (AMPfret signal) after addition of 20 mM 2-DG (blue) or vehicle (water; black). Data represent mean ± SEM (n = 3, about 140 cells per single experiment); * $p < 0.05$, ** $p < 0.001$ (two-way ANOVA test). (**d**) Microscopy images showing the non-normalized FRET ratio of AMPfret in a HaCaT C1 cell population at t = 0 min (T0) and t = 90 min (T90) from one representative experiment in (**c**). The AMPfret signal is given in a false color scale. (**e**) HPLC determination of ATP/ADP ratios in HaCaT C1 cells grown under conditions as used in FRET experiments, after a treatment with 20 mM 2-deoxyglucose (2-DG; blue) or vehicle (water; black) for 60 min. Data represent mean ± SEM (n = 3); ** $p < 0.001$ (unpaired Student's t-test). All scale bars represent 20 µm.

of glucose to 4.5 g/L alone for the 1 h culture period did not change them significantly. However, if high glucose culture was combined with Q10 preincubation, we observed a significant increase in all three energy parameters. Thus, glucose seems to enhance cellular energy status only after Q10 preloading, suggesting synergistic effects between both. All subsequent experiments were performed in high glucose medium.

Q10 preincubation protects keratinocytes energy state from oxidative stress

In the following, we investigated the effect of Q10 on the energy state of HaCaT C1 cells subjected to oxidative stress by utilizing the AMPfret biosensor. To increase intracellular Q10, HaCaT cells were preincubated with 30 µM Q10 for 24 h (Fig. 3a). Within the commonly used Q10 concentration range of 1–50 µM, which has been demonstrated to be safe and non-cytotoxic[36–40], we selected a concentration of 30 µM to facilitate rapid cellular uptake during the loading phase prior to the actual experiments. In the experimental setup for FRET experiments, HaCaT C1 cells were either preincubated with Q10 or vehicle alone before exposure to Luperox (tert-butyl peroxide), a potent organic peroxide capable of continuously generating free radicals[41] (Fig. 3b, c). Luperox addition consistently resulted in an increase in the AMPfret signal in all cells (Fig. 3b). However, in Q10-preincubated cells, this increase was slower and reached lower maximal levels during the observation period as compared to control cells (1.04 *vs* 1.10 for Q10 + Luperox *vs* vehicle + Luperox, respectively). Notably, the protective effect of Q10 became apparent as early as 12 min post-Luperox treatment and limited a further increase in AMPfret signal beyond about 60 min. In contrast, the AMPfret signal in untreated controls continued to rise throughout the entire observation period, albeit decelerating with time. The solvent vehicle alone did not alter the AMPfret signal compared to untreated HaCaT cells (Suppl. Figure 2a). Furthermore, when assessing cell viability, we found that Q10-loaded cells also maintained higher viability after Luperox treatment in comparison to the vehicle-treated controls (Suppl. Figure 2b). Thus, increased cellular Q10 levels can effectively attenuate detrimental Luperox effects by slowing the rate of oxidative insult on cell energetics, reducing its severity, and maintaining higher viability.

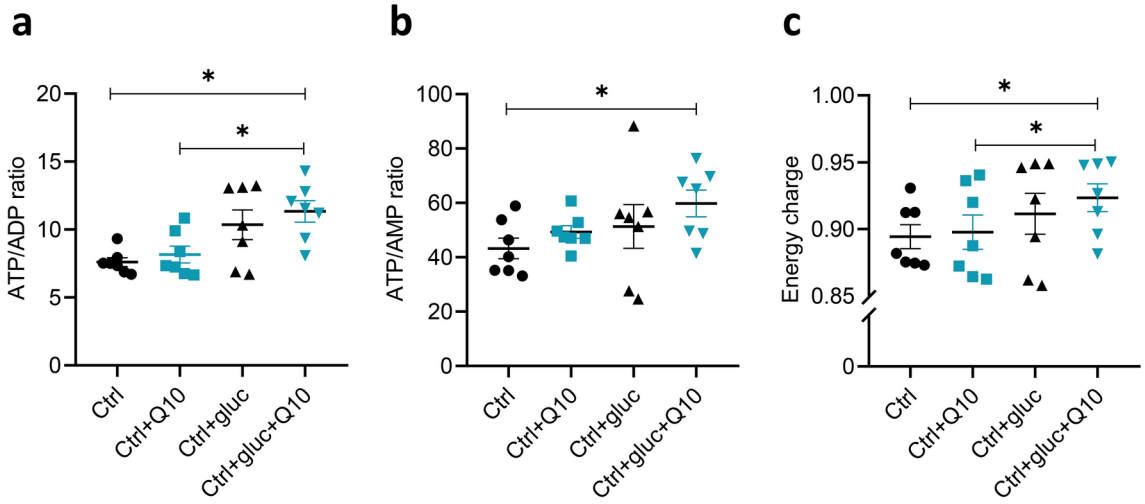

Fig. 2. Energy state parameters in HaCaT C1 keratinocytes supplemented with glucose and Q10. (**a**) ATP/ADP ratio, (**b**) ATP/AMP ratio, and (**c**) adenylate energy charge in HaCaT C1 cells either preincubated with 30 µM Q10 (blue) or vehicle only (black) in DMEM for 72 h, followed by transfer to a Q10-free medium containing either 1 g/L glucose (control) or 4.5 g/L glucose (+gluc) and cultured for 1 h. ATP, ADP, and AMP concentrations were quantified by HPLC. Data represent mean ± SEM (n = 7); * $p < 0.05$ (unpaired Student's t-test).

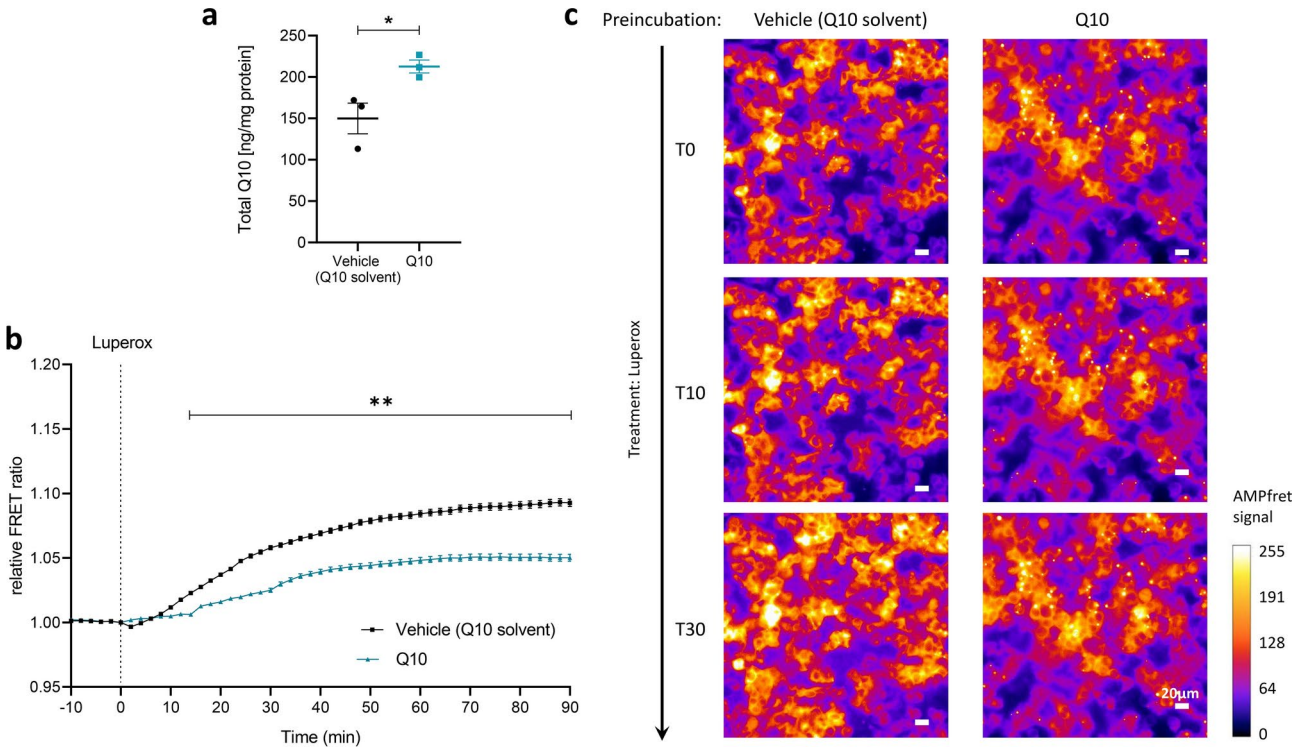

Fig. 3. Effect of Q10 preincubation on HaCaT C1 keratinocytes energy state under oxidative stress. (**a**) Q10 content of HaCaT C1 cells treated with 30 µM Q10 (blue) or vehicle (black) for 24 h. (**b**) Time course of normalized FRET ratio (AMPfret signal) of cells preincubated for 24 h with either 30 µM Q10 (blue) or vehicle only (black), and challenged with 1 mM Luperox at t = 0 min. Data represent mean ± SEM (n = 3, about 140 cells per single experiment); ** $p < 0{,}001$ (two-way ANOVA test). (**c**) Microscopy images showing the non-normalized FRET ratio of AMPfret in a HaCaT C1 cell population from one representative experiment in (b) preincubated for 24 h with 30 µM Q10 (right panels) or vehicle only (left panels), challenged with 1 mM Luperox at t = 0 min (T0), and further observed at t = 10 min (T10) and t = 30 min (T30). The AMPfret signal is given in a false color scale. The full time series can be found as movies 1 and 2 in supplementary data. All scale bars represent 20 µm.

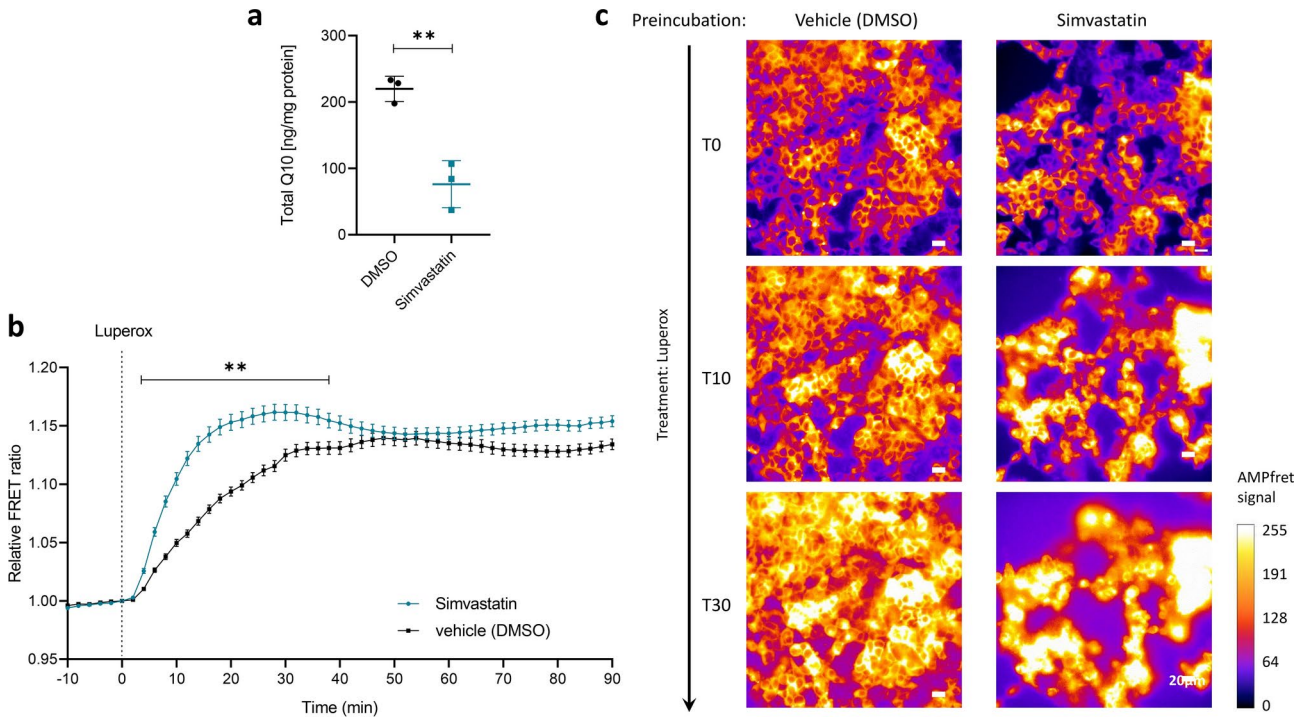

Fig. 4. Effect of Simvastatin preincubation on HaCaT C1 keratinocytes energy state under oxidative stress. (**a**) Q10 content of HaCaT C1 cells treated with 0.5 µM Simvastatin (blue) or vehicle (DMSO; black) for 48 h. Data represent mean ± SEM (n = 3); ** p < 0,001 (unpaired Student's t-test). (**b**) Time course of normalized FRET ratio (AMPfret signal) of cells preincubated for 48 h with either 0.5 µM Simvastatin or vehicle (DMSO), and challenged with 1 mM Luperox at t = 0 min. Data represent mean ± SEM (n = 3, about 140 cells per single experiment); ** p < 0,001 (two-way ANOVA test). (**c**) Microscopy images representing the non-normalized FRET ratio of AMPfret in a HaCaT C1 cell population from one representative experiment in (**b**), preincubated for 48 h with 0.5 µM Simvastatin (right panels) or DMSO vehicle only (left panels), and challenged with 1 mM Luperox at t = 0 min (T0), and further observed at t = 10 min (T10) and t = 30 min (T30). The AMPfret signal is given in a false color scale. The full time series can be found as movies 3 and 4 in supplementary data. All scale bars represent 20 µm.

Snapshots of a representative time course across of the AMPfret signal within a HaCaT cell population (Fig. 3c) and the corresponding movies (supplementary data) allow to appreciate the non-normalized responses of individual cells. First, the AMPfret signal of cells within the clonal population exhibited significant heterogeneity at baseline (t = 0 min), ranging from low to high intensity when categorized into classes of increasing FRET signal levels (Suppl. Figure 2c). However, there were significantly fewer cells with medium and high AMPfret signal in Q10 pretreated cells as compared to vehicle-only treated cells. These findings suggest that Q10 preincubation improves basal energy levels already independent of oxidative stress. Second, also the response to Luperox-induced oxidative stress exhibited marked heterogeneity. When the change in FRET signal after the first 30 min was categorized into classes of increasing FRET signal, responses ranged from non-responders to high responders in both Q10- and vehicle-pretreated cells. However, Q10 pretreatment largely increased the proportion of non-responders and low responders by 5- and threefold, respectively, while decreasing the number of mild responders by half (Suppl. Figure 2d). Moreover, individual cells that were already experiencing energy stress at baseline (t = 0 min), indicated by an appreciable FRET signal, also appeared to respond more readily to Luperox-induced oxidative stress. This variability may be attributed to differences in Q10 preloading, the cell's individual response to Luperox-induced oxidative stress, or a combination of both factors.

Inhibition of Q10 biosynthesis sensitizes keratinocyte energy state to oxidative stress

Next, we aimed to reduce intracellular Q10 pools by using Simvastatin, an inhibitor of the Q10-generating mevalonate pathway[42]. Simvastatin leads to Q10 depletion in mitochondria[43], and a concentration of 0.5 µM has no impact on the viability of HaCaT cell cultures for periods up to 48 h (Suppl. Figure 3a). Indeed, we observed that preincubation of HaCaT C1 cells with 0.5 µM Simvastatin for 48 h reduced cellular Q10 content by over 50% compared to DMSO vehicle only (Fig. 4a). We then reused the same experimental setup as above, in which HaCaT C1 cells were either preincubated with Simvastatin or vehicle for 48 h before being exposed to Luperox (Fig. 4b, c). Luperox addition resulted in an increase of the AMPfret signal in both conditions, but much faster in the Q10-depleted Simvastatin treated cells (Fig. 4b). Under these latter conditions, the AMPfret signal peaked at about 1.16 after only 30 min, which is close to the saturation level of AMPfret (unpublished). In vehicle-only control cells, the AMPfret signal peaked much later, close to 60 min, at a value of at 1.14, and

remained below the signal of Simvastatin treated cells. This indicates that inhibition of the mevalonate pathway, and the following cellular depletion of Q10, reduce the tolerance of the HaCaT energy state to endure oxidative stress. Snapshots of a representative AMPfret signal time course across the observed HaCaT cell population (Fig. 4c) and the corresponding movies (supplementary data) allow a more detailed appreciation of these data. Simvastatin-preincubated (Q10-depleted) cells reacted to Luperox not only by an increased AMPfret signal, but also by notable morphological changes and detachment from the culture dish, which are indicative of cell death. Indeed, Simvastatin treatment as compared to vehicle controls led to a strong decline in cell viability throughout the observation period (Suppl. Figure 3b). Regarding cell-to-cell variability of the FRET signal, we observed again considerable heterogeneity already at baseline before treatment, with Q10-depleted cells exhibiting a higher proportion of medium responses in the AMPfret signal compared to controls, indicating energy stress (Suppl. Figure 3c). Furthermore, the cell population again displayed heterogeneous responses to Luperox. When quantifying the change in AMPfret signal after the first 10 min, Q10-depleted cells had a fivefold higher share of high responders compared to the vehicle group (Suppl. Figure 3d). Taken together, an inhibited mevalonate pathway and resulting decreased cellular Q10 levels sensitize to detrimental Luperox effects, initially accelerating the oxidative insult on cell energetics, and rapidly leading to the onset of cell death.

Discussion

Q10 shows beneficial effects in stress protection and the treatment of various pathological conditions through its dual action of restoring electron flow in the respiratory chain and replenishing cellular antioxidant capacity[44]. Here, we conducted the first study applying a genetically-encoded FRET sensor of cellular energy state for a spatio-temporal analysis of Q10 effects under conditions of a harsh oxidative stress. Our model system, skin keratinocyte-derived HaCaT cells stably expressing the AMPfret biosensor, was validated for its capability to track real-time fluctuations in energy stress, i.e. reduced ATP/ADP and ATP/AMP ratios, as demonstrated earlier in other cell lines using transient transfection[23]. Q10 supplementation to human primary keratinocytes was already successfully shown to enhance cellular Q10 content and to improve cell energetics as measured by increased oxygen consumption rate[17,36]. Our study compared the effects of loading versus depleting Q10 on HaCat cells exposed to strong oxidative stress. It provides further insight into Q10 effects on keratinocyte cell energetics and viability:

First, Q10 loading of HaCaT cells was required to increase ATP/ADP and ATP/AMP ratios as well as adenylate energy charge in cultures at high glucose (4.5 g/L). This suggests that additional glucose needs an increased electron transfer capacity provided by Q10 to translate into higher mitochondrial ATP generation.

Second, AMPfret imaging with temporal and spatial resolution demonstrated protective effects of Q10 on HaCaT cell energetics. As a model, we applied harsh oxidative stress in form of Luperox, a peroxide that generates free radicals[41]. Following the onset of oxidative stress, Q10 preloading protected cells from a fast and strong decrease of cellular energy state, while the opposite was the case in Simvastatin treated cells, where Q10 depletion correlated with faster and more pronounced decline in energy state and rapid cell death. These data confirm, but also add substantial detail to what is known about the role of Q10 under conditions of oxidative stress[45]. In principle, Q10 can decrease the damage of oxidative stress on HaCaT cell energetics via different mechanisms, including stimulated cell respiration and antioxidative function[43]. Likely, both mechanisms participate in the protective effects reported here, since Q10 loading will increase both overall cellular Q10 and the Q10 pool involved in ETS.

Third, the AMPfret biosensor's ability to provide temporal resolution also at the single cell level identified marked cell-to-cell heterogeneity of energy state at baseline and in the Luperox-response. While such heterogeneity has been observed by FRET sensors in various other cellular systems[23,25–27], the causative mechanism remains to be determined. It may include differences in cell cycle, circadian rhythms, autonomous metabolic cycles or noise in gene expression[46]. Importantly, these cell population data provided evidence for Q10 loading already diminishing energy stress under basal conditions.

Our study emphasizes the role of Q10 in protecting keratinocytes from oxidative stress induced energy impairment. The significant protective effects observed here under strong oxidative stress conditions suggest that it may be also efficient under various forms of milder stress, such as detected e.g. with Q10 loading at baseline. Indeed, Q10's role in maintaining mitochondrial function and protecting against oxidative damage has preventive and therapeutic potential in various conditions characterized by mitochondrial dysfunction and oxidative stress[11,12]. Since our sensor reports cellular energy state, the major activator of AMPK, future research should focus on exploring links between Q10 and the AMPK signaling pathway, which is known to trigger antioxidative defense enzymes.

Material and methods

Cell culture, treatments and viability testing

HaCaT keratinocytes (addexBio) were transduced with lentiviral vectors coding for the three AMPfret subunits. Lentiviruses were produces by VectorBuildor (USA). Cells were selected 48 h post-infection with 1 µg/mL of puromycin (Invivogen) and 100 µg/mL of hygromycin B gold (Invivogen) for two weeks. Selection medium was changed every 3 days. Experiments with a validated HaCaT clone (C1) were carried out as described[26] with minor modifications. HaCaT cells were cultured in DMEM medium containing 4.5 g/L glucose, 10% FBS (Pan-Biotech), 50 µg/mL gentamycin (Gibco), and 100 U/mL penicillin and streptomycin (Gibco) in flasks and as well as onto a 2-well slide (IBIDI). The passage number of the HaCaT cells used in our experiments ranged from 15 to 28. For FRET experiments, replicates were performed using cells from different passages within this range. To achieve Q10 depletion, cells were preincubated for 48 h in DMEM supplemented with a final concentration of 0.5 µM Simvastatin (Sigma Aldrich), derived from a stock solution of 0.5 mM Simvastatin

in DMSO (Sigma Aldrich). Control cells were treated with vehicle only, using DMSO at the same dilution as that for the Simvastatin stock. For Q10 loading, cells were preincubated for either 24 or 72 h in DMEM supplemented with a final concentration of 30 µM Q10, using a stock solution of 23 mM Q10 (20 mg/mL, Kaneka Corporation) in Q10 solvent. The aqueous Q10 stock solution was generated by firstly dissolving Q10 in a mixture of glycerol (analytical reagent grade, Sigma Aldrich) and the emulsifier PEG-40 hydrogenated castor oil (HCO-40, BASF Personal Care and Nutrition) (Q10 : glycerol : PEG-40 0.4 : 0.6 : 1) and secondly diluting this solution with hot distilled water to 23 mM (w/v) Q10 according to Knott et al[17,47]. Control cells received the vehicle only, containing the same dilution of Q10 solvent as that for the Q10 aqueous stock solution. To maintain stability, the Q10 stock solution is stored at -20 °C in the dark to protect it from UV light exposure. Incubations with 10–50 µM Q10 are tolerated by keratinocytes, increase their cellular Q10 content, and improve their cell energetics as evidenced by enhanced oxygen consumption[17,36]. After preincubation, the DMEM medium was replaced with Fluorobrite medium containing either low glucose (1 g/L) or high glucose (4.5 g/L). Fluorobrite medium contains 10% FBS, 1 mM L-glutamine, 50 µg/mL gentamicin (Gibco), and 100 U/mL penicillin and streptomycin (Gibco). The slides were placed into the microscope incubation chamber (OKOLAB) at 37 °C, 5% CO2 and 95% humidity for 1 h to reach perfectly stable conditions. Then, either samples were taken for HPLC determination, or FRET image acquisition was started (see details below). After further 30 min (t = 0 min, T0), energy metabolism was perturbed by addition of the compound of interest: 20 mM 2-dexoyglucose (2-DG; glycolysis inhibitor) or the vehicle (water), or 1 mM Luperox (tert-butyl peroxide, an organic peroxide generating free radicals) or vehicle (DMSO). This relatively high concentration of Luperox was necessary to elicit a response within the 90-min observation period that allows for tracking of individual cells (unpublished). Likely, this requirement is due to the robust antioxidant machinery of HaCaT keratinocytes, which efficiently neutralizes reactive oxygen species[48]. For viability tests in parallel to FRET experiments, cells were seeded at a density of 0.5×10^6 in a 6-well plate and treated with 2-DG, Q10, Simvastatin or vehicle (DMSO, Q10 solvent, water) as described above. Viability was assessed at different time points by trypsinizing cells, centrifugating them at 200 × g for 5 min, mixing 20 µL of the cell suspension with 20 µL of trypan blue (Sigma Aldrich), and analyzing 10µL of the mixture in a cell counter (LUNA).

Image acquisition, analysis, and movie generation

Cells were observed by an epifluorescence microscope (Leica DMi8 equipped with HC PL APO 40X/0.95 dry objective) using an incubation chamber (see above). Fluorescence was excited by LED at 440 nm for CFP and 510 nm for Venus. Emission was collected for CFP (cyan) with BP filter 473 ± 11 nm plus a dichroic mirror at 460 nm, for Venus (yellow) with BP filter 539 ± 11 nm plus a dichroic mirror at 535 nm, and for the FRET channel with BP filter 473 ± 11 nm plus a dichroic mirror at 535 nm. Images were taken at a frequency of 1 picture every 2 min for 2 h. Exposure time was 100 ms and identical for each channel. For FRET analysis, the FRET SE module of the microscope software was used (Las X software, Leica). FRET ratio was calculated as described[26]:

$$FRETratio = \frac{fluorescence(ex : 473/22nm, em : 535nm)}{fluorescence(ex : 473/22nm, em460nm)}$$

The FRET ratio was derived within regions of interest corresponding to individual cells, with data from the entire cell population averaged and normalized to baseline values at the start of the treatment (t = 0 min, corresponding to 30 min after the start of image acquisition). FRET images and movies were generated by ImageJ software, using a home-made macro based on the PixFRET ImageJ plug-in described by Feige et al.[49]. A « Fire » LUT was applied using ImageJ to show the intensity levels of FRET ratio increase; color scale is given in the range of 0–256 (arbitrary units of grey levels). All image scale bars are 20 µm. For quantitative analysis of single cell heterogeneity within a cell population, raw AMPfret signals from individual cells at baseline (t = 0 min, before treatment) were normalized to the lowest signal within each experiment and categorized into three classes of increasing FRET signal levels: low (0–5% above population minimum), medium (5–10%) and high (above 10%). Single cell responses to Luperox were quantified by the difference in the raw AMPfret signal of individual cells between 0 and 30 min (for each Q10 experiment) or 0 min and 10 min (for each Simvastatin experiment). Signals were then categorized into four different classes of increasing FRET signal responses, defined as non-responders (< 1%), low responders (1–2%), medium responders (3–10%), and high responders (> 10%).

Protein extraction and immunoblotting

HaCaT C1 cells were homogenized in RIPA lysis buffer 1x, a ready-to-use solution containing 150 mM NaCl, 1.0% IGEPAL® CA-630, 0.5% sodium deoxycholate, 0.1% SDS, 50 mM Tris, pH 8.0. (Sigma Aldrich), and a protease inhibitor cocktail (Sigma Aldrich) and phosphatase inhibitors (Thermo Scientific). The supernatants obtained by centrifugation of homogenates (11,000 × g at 4 °C for 30 min) were collected and protein concentrations were determined using the micro-BCA protein assay (Intron Biotechnology) with a plate reader (Clario Star BMG LaBtech). Extracted proteins were mixed with 3 × blue loading buffer pack (Cell Signaling) supplemented with 42 mM DTT, and samples were heated at 95 °C for 5 min. Samples were then separated on 4–20% SDS-PAGE gels and transferred into 0.22 µm nitrocellulose membranes (Bio-Rad) using a Mini Trans-Blot Cell (Bio-Rad). The membranes were blocked in 5% non-fat dry milk-TBS Tween 0.05%, incubated overnight at 4 °C with antibodies (all rabbit, dilution 1:1000) against alpha2-AMPK, beta2-AMPK, and gamma1-AMPK (all from the AMPK Subunit Antibody Sampler Kit, Cell Signaling Technology, ref. #9839), washed, and then incubated for 1 h with horseradish peroxidase-labeled secondary antibodies (goat anti-rabbit, dilution 1:10,000, Jackson ImmunoResearch, ref. #111–035-00). Immunoreactivity was detected using chemiluminescence detection kit (Amersham). Bands were visualized using a LAS 4000 imager (GE Healthcare). Equal sample loading was verified with an anti-Pan-actin antibody (1:1000, Cell Signaling, ref. #111–035-00) used as internal control.

HPLC

Adenine nucleotides were determined in aqueous protein-free extracts using a high-performance liquid chromatograph (HPLC) (Varian 410, France) with a RP-C18 column (Polaris C18-A 4.6 × 250 mm, 5 µm, Varian, France; ref. A2000250R046) at a flow rate of 1 mL/min and a column temperature of 30 °C, as described in detail elsewhere[50]. Briefly, an initial seeding of 5×10^6 cells was performed in BP-100 dishes, followed by treatment. For extraction of adenosine nucleotides, cells were first washed three times with PBS and then lysed with 500 µL of 3.5% PCA (perchloric acid, 0.6 N). The extract was vortexed and then neutralized with 100–200 µL of K_2CO_3 (potassium carbonate, 5 M). The pH was verified using a pH paper (around 7). The neutralized solution was centrifuged at 12,000 × g for 5 min at 4 °C. The final protein free extract was stored at -80 °C until later analysis by HPLC. A protein-free extract (75 µl premixed with 50 µl mobile phase) was separated in pyrophosphate buffer (28 mM, pH 5.75) and elution followed by absorption at 254 nm. The elution peaks were integrated using the STAR software (Varian, France). ATP, ADP, and AMP concentration data were used to calculate ATP/ADP and ATP/AMP ratios, as well as the adenylate energy charge [(ATP + 0.5 × ADP) / (ATP + ADP + AMP)][35].

Cellular Q10 content

Cellular Q10 content was quantified from HaCaT C1 cells grown in 6-well plates as previously described[51]. Briefly, cell suspensions (approximately 500,000 cells) were extracted with isopropanol. After centrifugation, isopropanol extracts were analyzed by means of LC–MS/MS (Agilent 1200 HPLC coupled to an Agilent 6490 triple quadrupole mass spectrometer; separation column: YMC-Pack Pro C8 (YMC-Group)) using adjusted multi-reaction transitions and external standard calibration. Total Q10 content in HaCaT was normalized to total protein content analyzed by Pierce BCA Protein Assay Kit and expressed as ng Q10/mg protein.

Statistical analysis

Results are given as mean values ± SEM from three independent experiments unless stated otherwise. Statistical analyses were performed using the software Graphpad Prism 8. Student's t-test was used to test the significance of differences between control and experimental conditions (unpaired for between groups). For FRET analysis, data are expressed as mean ± SEM (n = 3, approximately 140 cells per experiment). Two-way ANOVA was used to perform multi-comparisons of one variable between at least three conditional samples (* $p < 0.05$, ** $p < 0.001$).

Data availability

The datasets generated during and/or analyzed during the current study are available from the corresponding author on reasonable request.

Received: 26 November 2024; Accepted: 15 April 2025
Published online: 25 April 2025

References

1. Jembrek, M. J., Orsolic, N., Karlovic, D. & Peitl, V. Flavonols in Action: Targeting Oxidative Stress and Neuroinflammation in Major Depressive Disorder. *Int. J. Mol. Sci.* https://doi.org/10.3390/ijms24086888 (2023).
2. Bentinger, M., Brismar, K. & Dallner, G. The antioxidant role of coenzyme Q. *Mitochondrion* **7**(Suppl), S41-50. https://doi.org/10.1016/j.mito.2007.02.006 (2007).
3. Acin-Perez, R., Fernandez-Silva, P., Peleato, M. L., Perez-Martos, A. & Enriquez, J. A. Respiratory active mitochondrial supercomplexes. *Mol. Cell* **32**, 529–539. https://doi.org/10.1016/j.molcel.2008.10.021 (2008).
4. Lenaz, G. & Genova, M. L. Structure and organization of mitochondrial respiratory complexes: A new understanding of an old subject. *Antioxid. Redox Signal.* **12**, 961–1008. https://doi.org/10.1089/ars.2009.2704 (2010).
5. Navas, P., Villalba, J. M. & de Cabo, R. The importance of plasma membrane coenzyme Q in aging and stress responses. *Mitochondrion* **7**(Suppl), S34-40. https://doi.org/10.1016/j.mito.2007.02.010 (2007).
6. Hyun, D. H., Hernandez, J. O., Mattson, M. P. & de Cabo, R. The plasma membrane redox system in aging. *Ageing Res. Rev.* **5**, 209–220. https://doi.org/10.1016/j.arr.2006.03.005 (2006).
7. Deshwal, S. et al. Mitochondria regulate intracellular coenzyme Q transport and ferroptotic resistance via STARD7. *Nat. Cell Biol.* **25**, 246–257. https://doi.org/10.1038/s41556-022-01071-y (2023).
8. Guerra, R. M. & Pagliarini, D. J. Coenzyme Q biochemistry and biosynthesis. *Trends Biochem. Sci.* **48**, 463–476. https://doi.org/10.1016/j.tibs.2022.12.006 (2023).
9. Wang, Y., Lilienfeldt, N. & Hekimi, S. Understanding coenzyme Q. *Physiol. Rev.* **104**, 1533–1610. https://doi.org/10.1152/physrev.00040.2023 (2024).
10. Xu, J. J. et al. Design of CoQ(10) crops based on evolutionary history. *Cell* https://doi.org/10.1016/j.cell.2025.01.023 (2025).
11. Cirilli, I. et al. Role of Coenzyme Q(10) in Health and Disease: An Update on the Last 10 Years (2010–2020). *Antioxidants (Basel)* https://doi.org/10.3390/antiox10081325 (2021).
12. Hernandez-Camacho, J. D., Garcia-Corzo, L., Fernandez-Ayala, D. J. M., Navas, P. & Lopez-Lluch, G. Coenzyme Q at the Hinge of Health and Metabolic Diseases. *Antioxidants (Basel)* https://doi.org/10.3390/antiox10111785 (2021).
13. Chang, K. H. & Chen, C. M. The Role of Oxidative Stress in Parkinson's Disease. *Antioxidants (Basel)* https://doi.org/10.3390/antiox9070597 (2020).
14. Tarry-Adkins, J. L. et al. Coenzyme Q10 Prevents Insulin Signaling Dysregulation and Inflammation Prior to Development of Insulin Resistance in Male Offspring of a Rat Model of Poor Maternal Nutrition and Accelerated Postnatal Growth. *Endocrinology* **156**, 3528–3537. https://doi.org/10.1210/en.2015-1424 (2015).
15. Blatt, T. & Littarru, G. P. Biochemical rationale and experimental data on the antiaging properties of CoQ(10) at skin level. *BioFactors* **37**, 381–385. https://doi.org/10.1002/biof.169 (2011).
16. Schniertshauer, D., Gebhard, D. & Bergemann, J. Age-Dependent Loss of Mitochondrial Function in Epithelial Tissue Can Be Reversed by Coenzyme Q(10). *J. Aging. Res.* **2018**, 6354680. https://doi.org/10.1155/2018/6354680 (2018).
17. Knott, A. et al. Topical treatment with coenzyme Q10-containing formulas improves skin's Q10 level and provides antioxidative effects. *BioFactors* **41**, 383–390. https://doi.org/10.1002/biof.1239 (2015).
18. Podda, M., Traber, M. G., Weber, C., Yan, L. J. & Packer, L. UV-irradiation depletes antioxidants and causes oxidative damage in a model of human skin. *Free Radic. Biol. Med.* **24**, 55–65. https://doi.org/10.1016/s0891-5849(97)00142-1 (1998).

19. Prahl, S. et al. Aging skin is functionally anaerobic: Importance of coenzyme Q10 for anti aging skin care. *BioFactors* **32**, 245–255. https://doi.org/10.1002/biof.5520320129 (2008).
20. Aaseth, J., Alexander, J. & Alehagen, U. Coenzyme Q(10) supplementation - In ageing and disease. *Mech. Ageing. Dev.* **197**, 111521. https://doi.org/10.1016/j.mad.2021.111521 (2021).
21. Tsujimoto, Y. Apoptosis and necrosis: Intracellular ATP level as a determinant for cell death modes. *Cell Death Differ.* **4**, 429–434. https://doi.org/10.1038/sj.cdd.4400262 (1997).
22. Pelosse, M., Cottet-Rousselle, C., Grichine, A., Berger, I. & Schlattner, U. Genetically Encoded Fluorescent Biosensors to Explore AMPK Signaling and Energy Metabolism. *Exp. Suppl.* **107**, 491–523. https://doi.org/10.1007/978-3-319-43589-3_20 (2016).
23. Pelosse, M. et al. Synthetic energy sensor AMPfret deciphers adenylate-dependent AMPK activation mechanism. *Nat. Commun.* **10**, 1038. https://doi.org/10.1038/s41467-019-08938-z (2019).
24. Crocker, H., Pelosse, M., Schlattner, U. & Berger, I. AMPfret: Synthetic nanosensor for cellular energy states. *Biochem. Soc. Trans.* **48**, 103–111. https://doi.org/10.1042/BST20190347 (2020).
25. Schmitt, D. L. et al. Spatial regulation of AMPK signaling revealed by a sensitive kinase activity reporter. *Nat. Commun.* **13**, 3856. https://doi.org/10.1038/s41467-022-31190-x (2022).
26. Abi Nahed, R. A. et al. FRET-based sensor for measuring adenine nucleotide binding to AMPK. *MethodsMol Biol*, **2882**, 15–45. https://doi.org/10.1007/978-1-0716-4284-9_2 (2023).
27. Schmitt, D. L. Imaging Subcellular AMPK Activity Using an Excitation-Ratiometric AMPK Activity Reporter. *Curr. Protoc.* **3**, e771. https://doi.org/10.1002/cpz1.771 (2023).
28. Frei, M. S., Mehta, S. & Zhang, J. Next-Generation Genetically Encoded Fluorescent Biosensors Illuminate Cell Signaling and Metabolism. *Annu. Rev. Biophys.* https://doi.org/10.1146/annurev-biophys-030722-021359 (2024).
29. Depry, C., Mehta, S., Li, R. & Zhang, J. Visualization of Compartmentalized Kinase Activity Dynamics Using Adaptable BimKARs. *Chem. Biol.* **22**, 1470–1479. https://doi.org/10.1016/j.chembiol.2015.10.004 (2015).
30. Miyamoto, T., Rho, E., Kim, A. & Inoue, T. Cellular Application of Genetically Encoded Sensors and Impeders of AMPK. *Methods Mol. Biol.* **1732**, 255–272. https://doi.org/10.1007/978-1-4939-7598-3_17 (2018).
31. Miyamoto, T. et al. Compartmentalized AMPK signaling illuminated by genetically encoded molecular sensors and actuators. *Cell Rep.* **11**, 657–670. https://doi.org/10.1016/j.celrep.2015.03.057 (2015).
32. Tsou, P., Zheng, B., Hsu, C. H., Sasaki, A. T. & Cantley, L. C. A fluorescent reporter of AMPK activity and cellular energy stress. *Cell Metab.* **13**, 476–486. https://doi.org/10.1016/j.cmet.2011.03.006 (2011).
33. Maschek, G. et al. 2-deoxy-D-glucose increases the efficacy of adriamycin and paclitaxel in human osteosarcoma and non-small cell lung cancers in vivo. *Cancer Res.* **64**, 31–34. https://doi.org/10.1158/0008-5472.can-03-3294 (2004).
34. Pelicano, H., Martin, D. S., Xu, R. H. & Huang, P. Glycolysis inhibition for anticancer treatment. *Oncogene* **25**, 4633–4646. https://doi.org/10.1038/sj.onc.1209597 (2006).
35. Atkinson, D. E. The energy charge of the adenylate pool as a regulatory parameter Interaction with feedback modifiers. *Biochemistry* **7**, 4030–4034. https://doi.org/10.1021/bi00851a033 (1968).
36. Staufer, T. et al. Assessing Cellular Uptake of Exogenous Coenzyme Q(10) into Human Skin Cells by X-ray Fluorescence Imaging. *Antioxidants (Basel)* https://doi.org/10.3390/antiox11081532 (2022).
37. Wieland, J. G. et al. Impact of Coenzyme Q(10) on Mitochondrial Metabolism: A Complementary Study Using Fluorescence Lifetime Imaging and Electron Microscopy. *Front. Biosci. (Landmark Ed)* **29**, 383. https://doi.org/10.31083/j.fbl2911383 (2024).
38. Kurashiki, T. et al. Molecular mechanisms underlying the promotion of wound repair by coenzyme Q10: PI3K/Akt signal activation via alterations to cell membrane domains. *J. Clin. Biochem. Nutr.* **70**, 222–230. https://doi.org/10.3164/jcbn.21-141 (2022).
39. Marcheggiani, F. et al. Anti-ageing effects of ubiquinone and ubiquinol in a senescence model of human dermal fibroblasts. *Free Radic. Biol. Med.* **165**, 282–288. https://doi.org/10.1016/j.freeradbiomed.2021.01.032 (2021).
40. Suntornnont, N., Kovavisarach, A. & Tammachote, R. Effects of Coenzyme Q10 on H2O2-Induced Oxidative Stress of Human Keratinocytes. *OBM Genetics* **09**, 279. https://doi.org/10.21926/obm.genet.2501279 (2025).
41. Herrera-Vaquero, M. et al. Signs of early cellular dysfunction in multiple system atrophy. *Neuropathol. Appl. Neurobiol.* **47**, 268–282. https://doi.org/10.1111/nan.12661 (2021).
42. Kitsugi, K. et al. Simvastatin inhibits hepatic stellate cells activation by regulating the ferroptosis signaling pathway. *Biochim. Biophys. Acta Mol. Basis Dis.* **1869**, 166750. https://doi.org/10.1016/j.bbadis.2023.166750 (2023).
43. Marcheggiani, F. et al. Modulation of Coenzyme Q(10) content and oxidative status in human dermal fibroblasts using HMG-CoA reductase inhibitor over a broad range of concentrations. From mitohormesis to mitochondrial dysfunction and accelerated aging. *Aging (Albany NY)* **11**, 2565–2582. https://doi.org/10.18632/aging.101926 (2019).
44. Littarru, G. P. & Tiano, L. Bioenergetic and antioxidant properties of coenzyme Q10: Recent developments. *Mol. Biotechnol.* **37**, 31–37. https://doi.org/10.1007/s12033-007-0052-y (2007).
45. Plecita-Hlavata, L., Jezek, J. & Jezek, P. Pro-oxidant mitochondrial matrix-targeted ubiquinone MitoQ10 acts as anti-oxidant at retarded electron transport or proton pumping within Complex I. *Int. J. Biochem. Cell Biol.* **41**, 1697–1707. https://doi.org/10.1016/j.biocel.2009.02.015 (2009).
46. Abbate, C. C., Hu, J. & Albeck, J. G. Understanding metabolic plasticity at single cell resolution. *Essays Biochem.* https://doi.org/10.1042/EBC20240002 (2024).
47. Failla, M. L., Chitchumroonchokchai, C. & Aoki, F. Increased bioavailability of ubiquinol compared to that of ubiquinone is due to more efficient micellarization during digestion and greater GSH-dependent uptake and basolateral secretion by Caco-2 cells. *J. Agric. Food Chem.* **62**, 7174–7182. https://doi.org/10.1021/jf5017829 (2014).
48. Hu, W. et al. Protective effects of isorhamnetin against H(2)O(2)-induced oxidative damage in HaCaT cells and comprehensive analysis of key genes. *Sci. Rep.* **13**, 2498. https://doi.org/10.1038/s41598-023-27575-7 (2023).
49. Feige, J. N., Sage, D., Wahli, W., Desvergne, B. & Gelman, L. PixFRET, an ImageJ plug-in for FRET calculation that can accommodate variations in spectral bleed-throughs. *Microsc. Res. Tech.* **68**, 51–58. https://doi.org/10.1002/jemt.20215 (2005).
50. Gratia, S. et al. Inhibition of AMPK signalling by doxorubicin: At the crossroads of the cardiac responses to energetic, oxidative, and genotoxic stress. *Cardiovasc. Res.* **95**, 290–299. https://doi.org/10.1093/cvr/cvs134 (2012).
51. Silvestri, S. et al. Coenzyme Q10 and alpha-lipoic acid: antioxidant and pro-oxidant effects in plasma and peripheral blood lymphocytes of supplemented subjects. *J. Clin. Biochem. Nutr.* **57**, 21–26. https://doi.org/10.3164/jcbn.14-130 (2015).

Acknowledgements

The authors are grateful to Stéphane Attia (LBFA, UGA Grenoble, France) for his support with adenylate determination. Tools used in this project were funded by the SATT Linksium, Grenoble, France and the French National Research Agency (project betaFRET, ANR-21-CE18-0060), and keratinocyte work was supported by Beiersdorf AG, Hamburg, Germany.

Author contributions

Conceptualization and experimental design: R.A.N., U.S., T.B., I.B, and J.M.W. Performed the experiments: R.A.N., A.H., C.C.R., F.A. and A.V. Data analysis: R.A.N. and U.S. Manuscript writing: R.A.N, J.M.W. and U.S.

All authors reviewed the manuscript.

Funding
SATT Linksium, Grenoble, France; Agence Nationale de la Recherche, betaFRET, ANR-21-CE18-0060, beta-FRET, ANR-21-CE18-0060; Beiersdorf AG, Hamburg, Germany.

Declarations

Competing interests
The authors declare no competing interests.

Additional information
Supplementary Information The online version contains supplementary material available at https://doi.org/10.1038/s41598-025-98793-4.

Correspondence and requests for materials should be addressed to R.A.N. or U.S.